Conference paper

Luca Fusaro*, Nikolay Tumanov, Giacomo Saielli and Riccardo Montis

Insights into the self-assembly of fampridine hydrochloride: how the choice of the solvent affects the crystallization of a simple salt

https://doi.org/10.1515/pac-2022-1208

Abstract: Crystalline materials and crystallization processes play an important role in several fields of science, such as pharmaceuticals, material science, pigments, optoelectronics, catalysis and energy storage. Understanding and defining the right conditions of crystallization is therefore crucial. Among the several factors influencing the crystallization of a given compound, the choice of the solvent system is perhaps one of the most important. The nature of solvent–solute interactions can indeed have a role in promoting specific molecular assemblies, therefore affecting crystallisation rates of a crystal and often resulting in the nucleation of different polymorphs and solvates. Here we investigated the role of a binary mixture of solvent (water/acetone) in the crystallisation of a simple salt of 4-aminopyridinium chloride. Previous results on this compound showed that when crystallised from water it forms a simple hydrate structure, while in the presence of acetone, it undergoes a liquid-liquid phase separation, followed by the crystallisation of a complex structure belonging to the Frank–Kasper (FK) phases, a particular family of topologically close-packed structures never observed in small and rigid molecules. To broaden the understanding of how such a simple molecule may crystallise as an FK phase, we carried out the crystallization of the complex phase by antisolvent diffusion (in a mixture of water/acetone) and that of the monohydrate phase in water, monitoring the liquid precursors by liquid-state NMR. In particular, we applied ^{1}H, ^{13}C, ^{14}N, ^{17}O, and $^{35/37}Cl$ NMR as a function of the concentration of $4APH^{+}Cl^{-}$ until the moment when precipitation of the crystalline phases occurred. Variations of chemical shifts, T_1 relaxation times of ^{13}C signals, and full-width at half-maximum of the signals of quadrupolar nuclei were also measured. The spatial proximity between the different species in the solution was investigated by NOE experiments. In order to support these results, we also performed Molecular Dynamics simulations, investigating the potential solute/solvents interactions. The results strongly suggest that acetone, instead of behaving as an anti-solvent, interacts directly with the solute, preventing the formation of the simple monohydrate structure and, at the same time, promoting specific molecular aggregations.

Keywords: Crystallisation; Italian-French NMR conference; liquid-state NMR; molecular dynamics; preferential solvation; solid-state NMR; X-ray diffraction.

Article note: A collection of invited papers based on presentations at the Italian-French International Conference on Magnetic Resonance, Milan, Italy, 27–30 September 2022.

***Corresponding author: Luca Fusaro**, NISM – Namur Institute of Structured Matter, University of Namur, 5000 Namur, Belgium, e-mail: luca.fusaro@unamur.be. https://orcid.org/0000-0001-5301-8034
Nikolay Tumanov, NISM – Namur Institute of Structured Matter, University of Namur, 5000 Namur, Belgium
Giacomo Saielli, CNR Institute on Membrane Technology Unit of Padova, Via Marzolo, 1 – 35131 Padova, Italy; and Department of Chemical Sciences, University of Padova, Via Marzolo, 1 – 35131 Padova, Italy. https://orcid.org/0000-0003-3337-8395
Riccardo Montis, Università degli Studi di Urbino Carlo Bo, Via della Stazione 4, I-61029 Urbino, Italy

© 2023 IUPAC & De Gruyter.

Introduction

"Like dissolves like". This simple statement represents a rule of thumb to choose the suitable solvent for a given solute. It is based on the assumption that substances with similar polarity dissolve one into the other, as the consequence of favourable solute-solvent intermolecular interactions.

The choice of the right solvent for a given solute is an important step for several processes, such as organic synthesis, purification methods and crystallisations. In the industrial and technological sectors, crystalline materials are applied in gas storage, optoelectronics and, in particular, in the pharmaceutical field, where crystallization techniques are crucial for purification and separation processes when manufacturing active pharmaceutical ingredients (APIs), as well as for screening and designing new solid forms with improved physicochemical properties [1].

Although sublimation [2] and melt cooling [3] represent viable methods for crystallization, those from solution are certainly the most common. The choice of the solvent plays an important role in the outcome of nucleation and crystal growth. Solvent–solute interactions can indeed promote specific molecular assemblies, resulting in the nucleation or growth of different polymorphs and solvates or simply affecting nucleation and growth rates of a crystal [4].

In general, when a compound is dissolved in a mixture of two solvents, the solute is expected to interact mainly with the component that forms the strongest solute-solvent interactions. A typical example of this case is the crystallisation by the so called "antisolvent" diffusion, a common procedure to induce a decrease of the solubility of a solute in a solution, favouring supersaturation and therefore promoting the nucleation or the crystallisation of the target compound [5]. In this case, the solute is intuitively expected to be preferentially (or selectively) solvated by the solvent, being the antisolvent part of the outer solvation sphere, generating a non-uniform composition and therefore regions of high supersaturation [6].

The term preferential solvation is often used to define the case when the local composition of solvents in the immediate proximity of the solute (the cybotactic region) is different when compared to the bulk composition [7]. This phenomenon is further complicated by the micro-heterogeneity of the solution itself, which may present a complex, locally heterogeneous structure, as reported for aqueous mixtures of common solvents as acetonitrile, DMSO, acetone, etc. [8–11].

The nature of such complex interactions between solute and mixtures of solvents may be investigated by both computational and experimental techniques. Classical molecular dynamics simulations (MD) can be applied to investigate the nature of molecular clusters and micro-heterogeneities in solution, via the analysis of radial distribution functions (RDF) and spatial distribution functions (SDF) [12]. On the other hand, NMR spectroscopy, and specifically the Nuclear Overhauser Effect (NOE), which is based on the dipolar interaction between spatially-close spins, may provide experimental information on solute-solvent interactions [7, 13].

In a recent article, we reported on the structural characterisation of a family of salts of 4-aminopyridinium chloride ($4APH^+Cl^-$), also known as fampridine hydrochloride [14]. This system produced four different phases: two complex Frank–Kasper (FK) A15 sub-hydrate phases (**1** and **2**), a simple monohydrate phase (**3**), and a simple anhydrous phase (**4**).

Phases **2** and **4** were both obtained by crystallisation from the melt, while **1** and **3** were crystallised from solutions. In particular, the monohydrate **3** (see Fig. 1b) was crystallised by solvent evaporation from a supersaturated aqueous solution (labelled as **L3**), producing plate-like crystals. The complex phase **1** (Fig. 1a) was obtained from a dense liquid phase (DLP) (labelled as **L1**) separated from a solution of $4APH^+Cl^-$ in a water and ethanol mixture, after adding acetone as the antisolvent. A further addition of acetone promoted the formation of block-like crystals of the complex sub-hydrate **1**. This structure, very similar to the other sub-hydrate **2**, showed a very complex self-assembly in solid state, consisting of three different polyhedral clusters of Cl^- and $4APH^+$ packed together in a fashion resembling that observed in clathrate hydrates [15].

Such a complexity in the solid state was explained as the result of a specific and complex preorganisation in the liquid phase **L1**, that, at the same time, prevented the crystallisation of the monohydrate **3**.

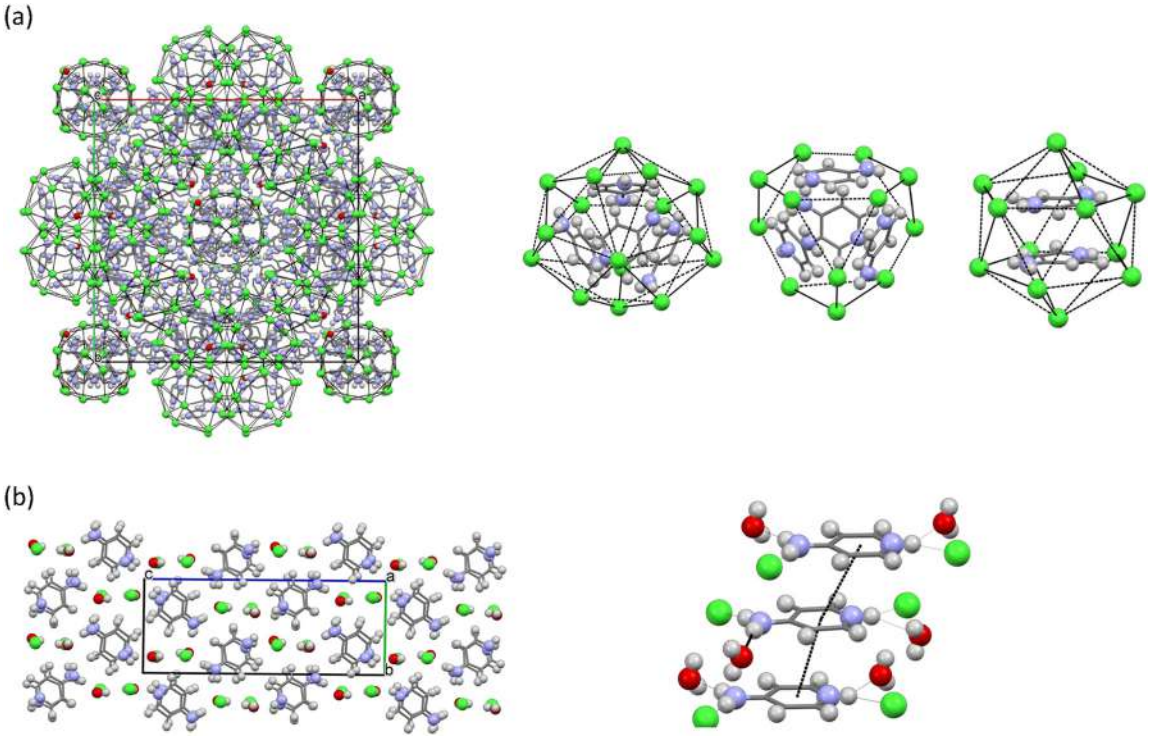

Fig. 1: Crystal packing of crystalline phases **1** (a) and **3** (b), viewed along the same axes of the unit cell (left) and main self-assemblies of the same phases (right) [14].

The crystallisation of **1** from the dense liquid phase **L1** was monitored by NMR and the results compared with those obtained for **3** from the aqueous solution **L3**. The results showed differences in composition, chemical shifts, ^{13}C relaxation time, and full width at half maximum (FWHM) of selected resonance lines, confirming that the dramatic differences in the solid state between **1** and **3** must be ascribed to a significantly different preorganisation in the precursor liquid phases **L1** and **L3**. In particular, a cryo-EM analysis of **L1**, showed spherical aggregates with size consistent with those observed in the crystal structure **1** [14].

Although these complex phases might be regarded simply as a curious case, understanding and controlling their formation and the reasons of such a complex self-assembly in the liquid state is crucial to extend these results to other systems, opening the way for the design of a new class of crystalline materials.

In this work we investigated the potential role of preferential solvation and solute-solvent interactions in promoting the crystallisation of such complex crystal structures. In order to simplify the study, we limited our investigation to a bi-component solvent system. For this purpose, instead of crystallising $4APH^+Cl^-$ by acetone diffusion from a mixture water/ethanol, we attempted to prepare **1** from water, upon addition of acetone as the antisolvent. The resulting liquid phase was then fully characterised by liquid state NMR. Solid-state NMR and powder X-ray diffraction (PXRD) were used to characterise the products of crystallisation. Finally, molecular dynamics simulations were performed to provide an interpretation to our experimental results.

Results and discussion

LLPS and crystallisation

Firstly, we performed a crystallisation of **1** from H_2O, upon addition of acetone as the anti-solvent. The procedure was adapted from that previously reported for the preparation of **1** [14]. Accordingly, solid 4AP was dissolved in concentrated HCl, and progressive additions of acetone induced a liquid-liquid phase separation (LLPS, see Fig. 2)

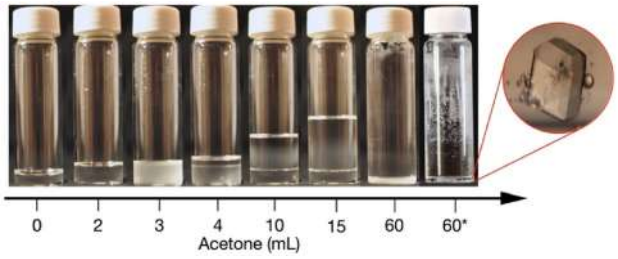

Fig. 2: Crystallisation of 4APH$^+$Cl$^-$ in water and acetone. The asterisk indicates the sample where crystallisation occurred.

resulting in a supernatant and a dense liquid phase (DLP). Further addition of acetone to the system, resulted in the precipitation, after approximately 24 h, of block-like crystals. The variation in composition of the DLP (labelled as **L1***), upon addition of acetone was monitored by ^{1}H NMR, showing an analogous behaviour to that previously reported for **L1** [14]. This suggested that the crystallisation from a concentrated DLP composed by water and acetone might produce again a complex phase. This crystalline sample was studied by powder X-ray diffraction. Although the results were clearly consistent with a complex phase, we could not unequivocally identify whether the structure corresponded to **1**, **2** or to a new sub-hydrate FK phase.

To better understand the molecular behaviour of cations, anions, and their interactions with the two solvents, we prepared **L1*** on a larger scale (see experimental) and monitored the sample upon addition of acetone, until crystallisation occurred. We characterised the **L1*** samples after each addition of acetone by ^{1}H, ^{13}C, ^{14}N, ^{17}O, ^{35}Cl and ^{37}Cl NMR experiments.

Multinuclear NMR in solution

Selected ^{1}H NMR spectra of **L1*** are shown in Fig. 3a and b, while a larger selection of spectra can be found in Supporting Information. Sharp resonance lines were observed for CH moieties of 4APH$^+$, as well as for the CH_3 groups of the acetone molecule. A broad resonance line was observed for the NH group, due to the J-coupling with ^{14}N. Also, the signals of the water and NH_2 group of 4APH$^+$ were significantly broadened, due to the chemical exchange (see Supporting Information). After addition of each aliquot of acetone, significant variations of the integrated areas and chemical shifts were observed.

The analysis of the composition of **L1***, upon each addition of acetone, showed that, while the amount of water continued to decrease steadily (Fig. 3c), the concentration of acetone reached a plateau. In particular, the

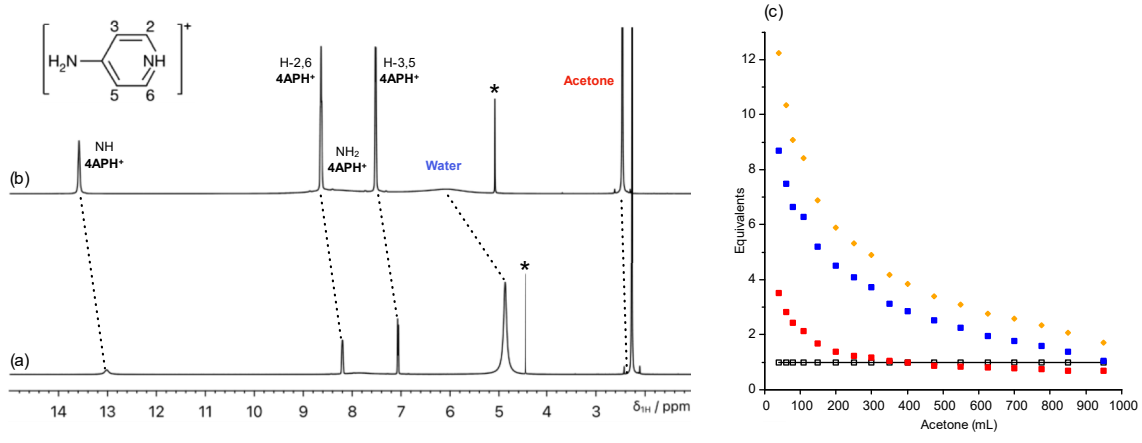

Fig. 3: ^{1}H NMR spectra of **L1*** immediately after the LLPS (a) and before the crystallisation (b) and assignments of the NMR resonances. (c) Variation of the amount of acetone (■), water (■), and the total amount of solvents (◆) with respect to 4APH$^+$ (□). The asterisks (*) indicate the residual peak of HDO present in the coaxial insert.

composition of the highest concentrated sample, obtained just prior the formation of crystals of the complex phase, showed 1.00 equivalent of $4APH^+Cl^-$, 1.04 equivalent of H_2O and 0.68 equivalents of acetone. These results suggest a possible role of acetone in the stabilisation of $4APH^+Cl^-$ in **L1*** and are in great agreement with those previously reported for **L1**. Indeed, as in the case of **L1**, the crystallisation of $4APH^+Cl^-$ from **L1*** was again observed when the total amount of solvents in the DLP was lower than 2 equivalents.

We previously interpreted this behaviour considering that the addition of acetone promotes a specific pre-organisation of the $4APH^+Cl^-$ ion pairs in the DLP allowing the crystallisation of **1** and, simultaneously, preventing the nucleation of the monohydrate **3**. $4APH^+Cl^-$ is weakly soluble in acetone and we expect that, in **L1***, the salt would be preferentially or exclusively solvated by H_2O, being the acetone micro-segregated or part of the outer solvation sphere.

To evaluate the behaviour of acetone in the DLP, we characterised a concentrated sample of **L1*** by 2D NOESY NMR experiments at 25 °C. NOEs strongly depend on $\omega\tau_c$ (where ω is the Larmor frequency and τ_c is the correlation time of the species under investigation). In particular, when $\omega\tau_c$ values are close to 1, the resulting NOEs are close to zero [16]. In general, NOEs are strongly affected by the dynamics of the molecules in solution and therefore depend on the molecular size and on the viscosity of the system. Generally, positive NOEs are observed for small molecules while larger molecules show negative values.

When the 2D NOESY experiment was recorded at 25 °C, no significant intermolecular cross peaks were observed. This might be due either to the relatively high viscosity of the DLP, that decreases the dynamics of the molecules in solution, or to the absence of any interaction between acetone molecules and $4APH^+Cl^-$.

In order to investigate the potential interactions of acetone with $4APH^+Cl^-$ in more detail, we decreased the temperature to 5 °C and performed a further 2D NOESY experiment. The results show negative intra- and intermolecular cross-peaks (see Fig. 4a). Interestingly, relatively intense cross-peaks between the signal of CH_3 groups of acetone and the aromatic CH signals of the cation were observed, suggesting that acetone interacts to $4APH^+Cl^-$ moieties and is part of their solvation sphere. Increasing the vertical scale, a negative cross peak was observed also between the CH_3 signal of acetone and the NH signal of the cation. Similarly, broad negative cross-peaks were also observed between the water and NH_2 signals, which experience a chemical exchange (see Supporting Information).

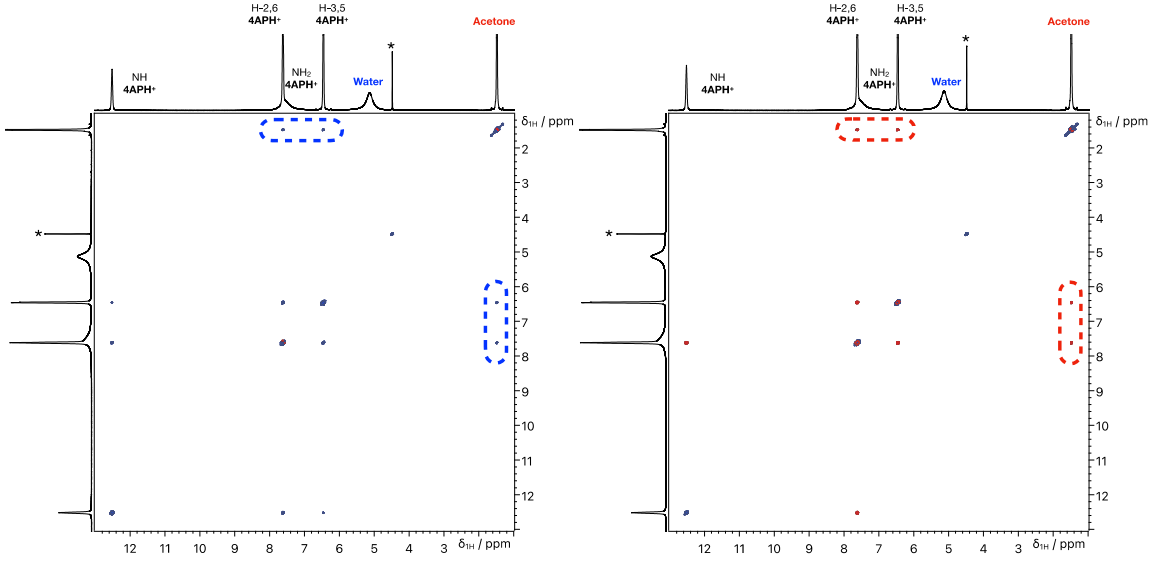

Fig. 4: ^{1}H NMR experiments of a concentrated DLP recorded at 5 °C: phase-sensitive 2D NOESY obtained with a mixing time of 500 ms (left), and 2D ROESY obtained with a mixing time of 200 ms (right). The intermolecular cross-peaks between the signal of CH_3 groups of acetone and CH signals of the cation are highlighted. The blue signals are phased negative, while those red are positive. The asterisk (*) indicate the signal of residual peak of HDO present in the coaxial insert.

In addition to 2D NOESY NMR experiments, we characterised the DLP by Rotating-frame Overhauser Effect SpectroscopY (ROESY) 2D experiments, analysing **L1*** at 5 °C. Differently to NOESY, ROESY experiments provide positive cross peaks for all the spatially-close ^{1}H atoms, while diagonal-peaks as well as the cross-peaks due to chemical exchange are negatively phased, irrespectively of the correlation time of the species under study. The results of the 2D ROESY experiments at 5 °C show relatively intense positive cross-peaks between the CH_3 groups of acetone and the CH group of the cation (see Fig. 4b), and negative cross-peaks between NH_2 and water, as a consequence of the chemical exchange (see Supporting Information) [16].

The chemical shift variation ($\Delta\partial$) of ^{1}H signals of the cation, water and acetone was monitored as a function of the $4APH^+Cl^-$ molar fraction (X_{4APH}), showing large and positive values. This indicates that all the signals are in fast exchange on the chemical shift timescale. The observed shift to higher frequencies is assigned to the presence of stronger H-bonds at higher salt concentration [17].

The $\Delta\partial$ of the signals not affected by chemical exchange are reported in Fig. 5a. Interestingly, while the signals assigned to $4APH^+$ cation show mainly linear shifts at increasing X_{4APH+} values, the signal of acetone shows a different trend. Indeed, its variation of chemical shift appears to be non-linear, initially increasing and eventually reaching a plateau. One possible explanation for this observation is that at high X_{4APH+} values, acetone molecules might be in a bound-like state, interacting with water and $4APH^+Cl^-$ and forming a particular type of aggregate.

The $\Delta\partial$ of ^{1}H signals that experience a chemical exchange are shown in Fig. 5b. Large and positive chemical shift variations are observed as a function of X_{4APH+}. These reach maximum values of approximately 1.2 and 0.6 ppm for water and NH_2 signals, respectively. At the highest X_{4APH+} values, the $\Delta\partial$ variation deviates from linearity, probably because those signals are in a chemical exchange and close to coalescence.

Although there is an open debate on the sensitivity of NOE-based experiments to intermolecular solute-solvent interactions [18, 19], we believe our results show strong evidence that acetone is part of the cation solvation shell. This is also supported by molecular dynamics calculations (see below). In particular, we believe that, similarly to what observed in our previous study, as the concentration of the DLP increases, $4APH^+Cl^-$ must be aggregated. Furthermore, our results suggest that these aggregates are not preferentially solvated by water molecules but also contain acetone in their first solvation sphere.

In order to gain a deeper comprehension of the behaviour of cation, anion and solvent molecules, we recorded heteronuclear NMR spectra of quadrupolar nuclei as ^{14}N, $^{35/37}$Cl, and ^{17}O. These spectra are expected to provide different information, based on their environment and dynamics. Indeed, we expect that, similarly to the ^{1}H chemical shifts, also those of heteronuclei would be generally sensitive to the change of composition, and hence of the solvation shell of the different species in solution. Furthermore, the increase of viscosity would induce

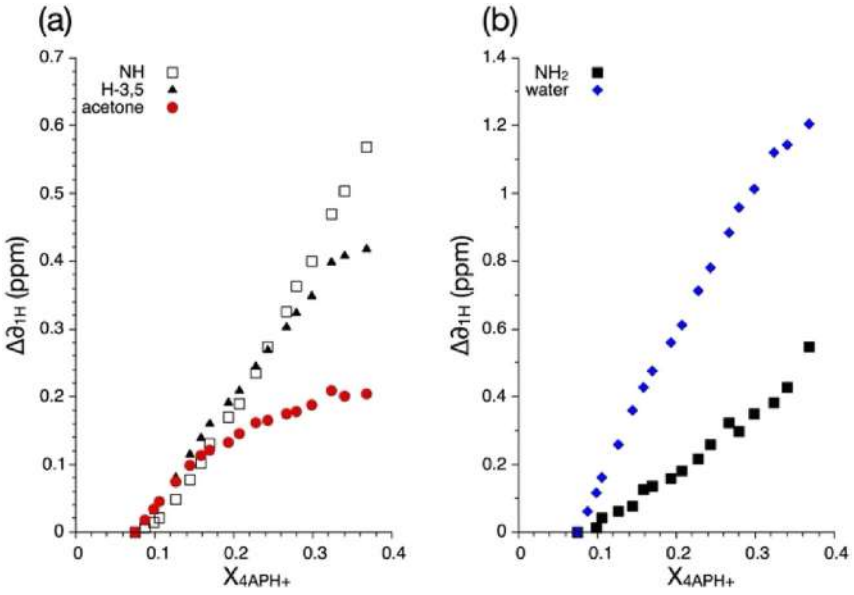

Fig. 5: ^{1}H chemical shift variation as a function of X_{4APH+} of (a) NMR signals not affected by chemical exchange, (b) NMR signals affected by chemical exchange.

slower dynamics of atoms/molecules, inducing faster quadrupolar relaxation and consequently broadening the signals. For this reason, both the chemical shift variations and the full width at half maximum (FWHM) values of the signals of quadrupolar nuclei were analysed.

Figure 6 shows selected ^{35}Cl, ^{17}O and ^{14}N spectra of DLP samples collected immediately after the LLPS (bottom) and prior the crystallisation (top). The complete series of spectra is reported in Supporting Information. The signal of the anion was easily observed by $^{35/37}$Cl NMR, also at higher X_{4APH+} values. On the contrary, the observation of the water signal was limited by the low ^{17}O natural abundance (0.037 %). ^{17}O-enriched water was then added to the mother solution to decrease the instrumental time needed to record the spectra. A different situation occurred in the case of ^{14}N spectra: the NH signal was easily observed also at higher X_{4AP} values. However, the resonance line of NH_2 moiety was not detected at higher X_{4AP} values, because of severe broadening due to larger electric field gradients (EFG) [20].

Both the $^{35/37}$Cl NMR and ^{17}O signals display large variations of chemical shift values ($\Delta\partial$ is 20 and 12 ppm, respectively) as a function of X_{4APH+} (see Figs. 6a,b and 7a). On the contrary, the ^{14}N signal of NH group does not show significant $\Delta\partial$, even at higher X_{4AP} values (see Fig. 6c). This is expected, as every change in composition will induce some change in the first sheath of water and chloride. On the contrary, any change in the composition would not significantly affect the local environment of the nitrogen atoms [21, 22].

FWHM values of all the quadrupolar nuclei under scrutiny are extremely sensitive to changes in the composition (see Fig. 7b). In general, increases in the concentrations produce broader signals, as expected for solutions which become macroscopically more viscous.

The ^{14}N signal of NH_2 of the cation is the broadest, having FWHM comprised between 2 and 19 kHz. The FWHM of NH signal is significantly sharper, ranging between 450 and 3800 Hz. Those values were estimated by a deconvolution analysis of the resonance lines, which are broad and superimposed. Further details about the deconvolution analysis are provided in Supporting Information.

The ^{35}Cl and ^{37}Cl signals of the anion show the same trend. As expected, ^{37}Cl provide less intense but sharper resonance lines, in agreement with their respective natural abundance and quadrupole moment [23]. Their

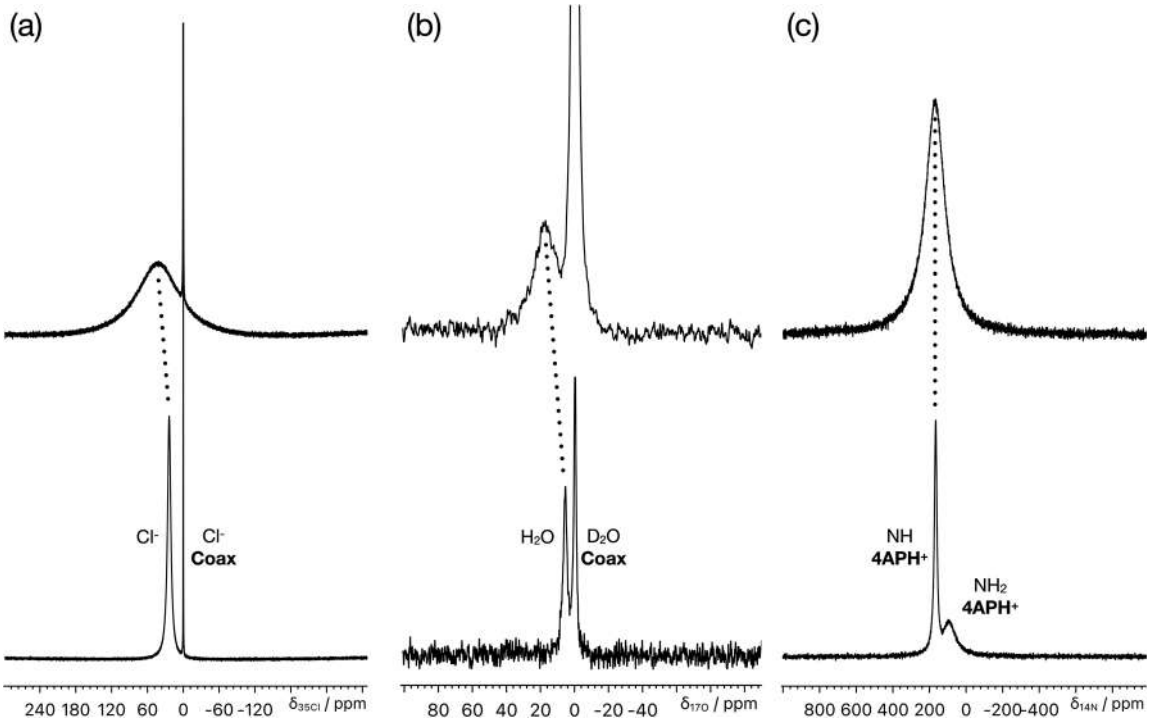

Fig. 6: ^{35}Cl, ^{17}O, and ^{14}N NMR spectra of DLP samples collected immediately after the LLPS (bottom) or before the crystallisation (top).

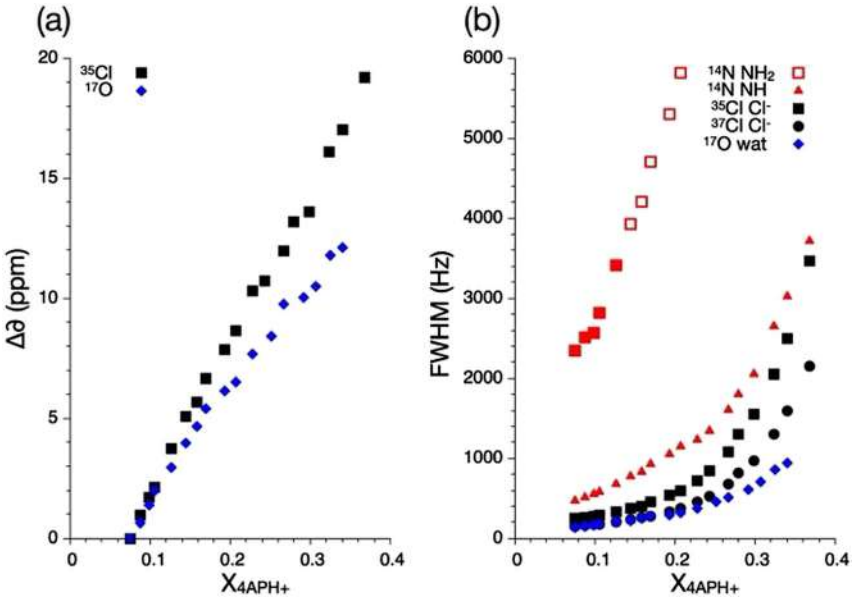

Fig. 7: Variation of (a) chemical shift values of resonance lines of quadrupolar nuclei, and (b) full width at half maximum (FWHM) of resonance line of quadrupolar nuclei, as a function of the 4APH$^+$ molar fraction. The open symbols (■) indicate the FWHM values of broad ^{14}N signals obtained by deconvolution.

FWHM generally lie between 150 and 3500 Hz. The water signal detected by ^{17}O was the sharpest among the quadrupolar nuclei, being FWHM comprised between 130 and 950 Hz.

We then compared the results relative to **L1*** (this work) with those previously reported for **L1** and **L3** [14].

Figure 8a and b shows the ^{1}H chemical shift variation of the NH and H-3,5 signal in **L1**, **L1***, and **L3** samples. The comparison of the NH signal for the three samples shows significant differences. These are particularly large at low concentrations of 4APH$^+$Cl$^-$. As described in our previous paper, the differences between **L1** and **L3** are particularly marked and were ascribed to the different solvent composition. This is due to the fact that the NH chemical shift is sensitive to the presence of both ethanol and acetone. This also explains the differences observed between **L1** and **L1*** at low concentrations of 4APH$^+$Cl$^-$. When the concentration increases, the amount of EtOH in **L1** is rather low and consequently, **L1** and **L1*** are similar in chemical composition and show similar NH chemical shift values.

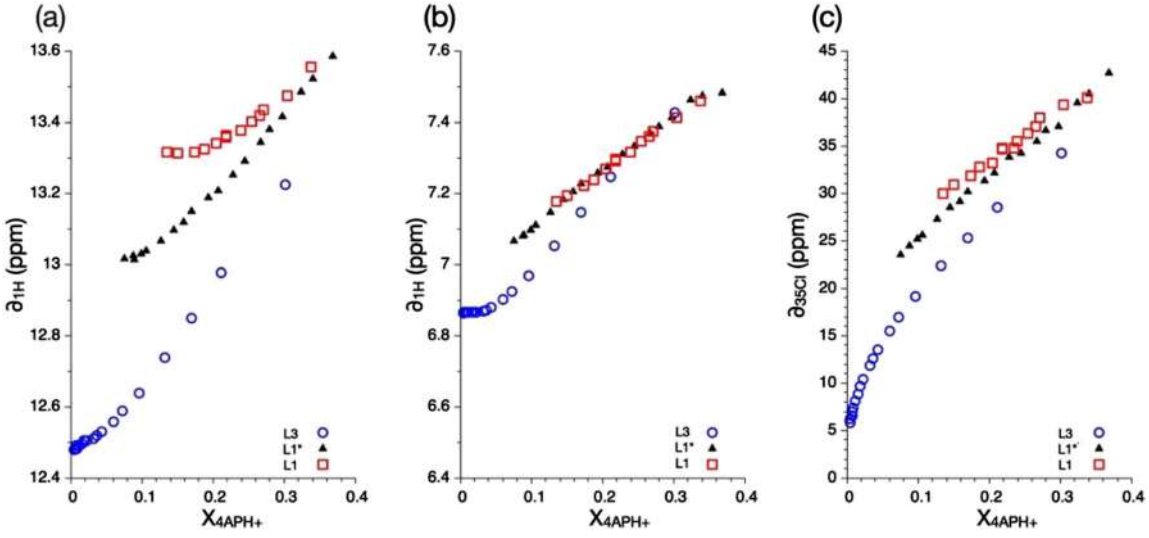

Fig. 8: Comparison of the results obtained for **L1**, **L1*** and **L3*** as a function of the 4APH$^+$ molar fraction: ^{1}H chemical shift of NH signals (a) ^{1}H chemical shift of H-3,5 signals (b) and ^{35}Cl chemical shift of chloride anion. **L3** and **L1** results were obtained from aqueous and water/ethanol/acetone solution and reported previously [14].

The analysis of the chemical shift variation of the H,3-5 signals as the function of the X_{4APH+}, i.e., the main intermolecular signal appeared in 2D NOESY/ROESY experiments, shows a similar behaviour for **L1** and **L1***. In the case of **L3**, the behaviour is different at low concentrations and converges to **L1** and **L1*** when the concentration increases, probably because the direct interaction between H-3,5 and chloride anions in all the samples (see Fig. 8b). Finally, also the ^{35}Cl chemical shift appear to be closer in **L1** and **L1***. Its value is generally larger than those obtained for **L3** (see Fig. 8c).

The comparison of the FWHM of signals of quadrupolar nuclei and ^{13}C T_1 relaxation time provides some dynamic information. The ^{35}Cl FWHM measured for **L1*** as the function of the molar fraction of $4APH^+Cl^-$ (see Fig. 9a) is intermediate between that measured for **L3** and **L1**, suggesting that the viscosity of **L1*** should follow the same trend. To verify this hypothesis, we measured the ^{13}C T_1 relaxation time of CH signals. These are expected to result only from intramolecular dipolar coupling to directly attached protons and rotational correlation time of the cation [24] and, consequently, to the viscosity of the solution. Also in this case, the behaviour of, **L1*** is intermediate between **L3** and **L1** (see Fig. 9b), confirming that, at low concentrations of $4APH^+Cl^-$, the viscosity of the three systems varies as follow: **L3** < **L1*** < **L1**.

At molar fractions of $4APH^+Cl^-$ close to 0.3, the ^{13}C T_1 relaxation time of CH signals of **L1**, **L1*** and **L3** converge to a similar value, just prior the nucleation takes place. Assuming similar viscosities for the three samples at this concentration, the large difference in the FWHM of the ^{35}Cl signals measured for **L3**, **L1** and **L1*** must be ascribed to differences in the local environment of chlorides, i.e., to larger EFG in presence of acetone (and ethanol). These results confirm that ^{35}Cl is extremely sensitive to its local environment, able to probe subtle changes induced by the proximity of different solvents [21].

The crystalline phases obtained in this work were also analysed by solid state (SS) techniques as SSNMR and powder X-ray diffraction. The results are compared with those obtained for samples of **1** and **3**.

SSNMR

TOtal-Sidebands-Suppression (TOSS) ^{13}C NMR spectra were recorded at 14.1T and room temperature on crystalline phases nucleated from **L1**, **L1*** and **L3**. The spectrum of the monohydrate **3** obtained from **L3** shows multiple signals, as expected for samples with Z′ > 1 [25]. In this case, Z′ is 4, and we would expect to observe up to eight signals for the C-2,6 and C-3,5, respectively. However, due to their superimposition, the signals cannot be easily discriminated (see Fig. 10a). Three distinct C-2,6 signals are however observed, and this is in some way consistent

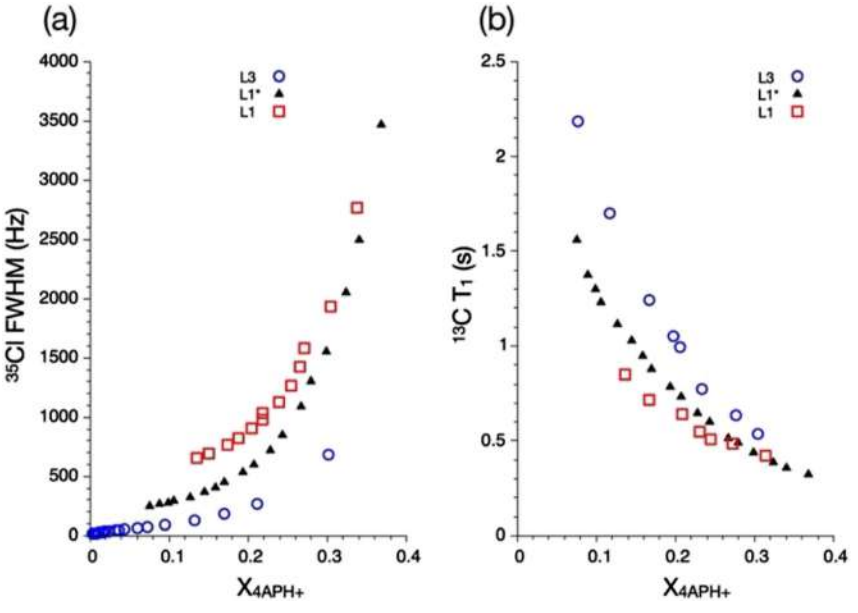

Fig. 9: Comparison of the results obtained for **L3**, **L1** and **L1*** as a function of the $4APH^+$ molar fraction: FWHM of ^{35}Cl signals (a) and ^{13}C T_1 relaxation time (b).

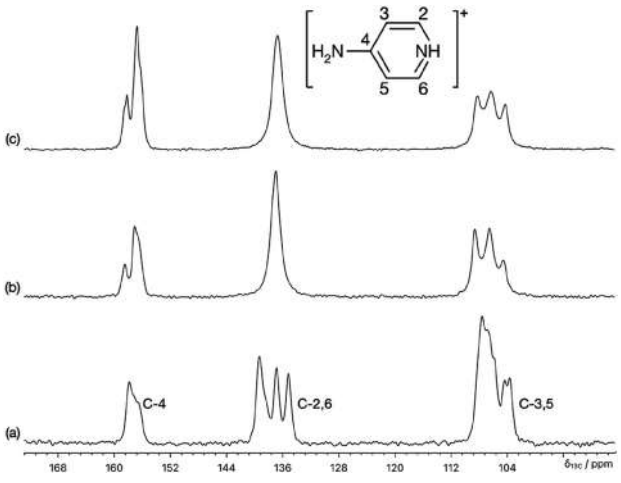

Fig. 10: ^{13}C TOSS CP-MAS NMR spectra of 4APH$^+$Cl$^-$ recorded at 14.1T and room temperature: Monohydrate phase **3** (a), complex phase **1** (b), sample prepared in this work from **L1*** (water/acetone) liquid precursor (c).

with what observed in the crystal structure of the monohydrate **3**, where the environment of those atoms is affected by the different interactions with chloride, water and the presence of adjacent 4APH$^+$ moieties.

This is also confirmed by the observation that, in the case of the complex phase **1**, the same signal was not resolved into different contributions (see Fig. 10b). In this case, all the C-2,6 interact only with Cl$^-$ anions. Indeed, the CH signal are always found in hexagonal or pentagonal tiles, interacting directly with chloride anions, where dramatic variations of chemical shift values are not expected.

The ^{13}C NMR spectra of the solid phase crystallised in this work from **L1*** is clearly similar to the spectrum of the complex phase previously reported (see Fig. 10c). No signals of the monohydrate phase were detected, confirming that acetone and water are sufficient to promote the complex self-assemblies that produces the FK phases of 4APH$^+$Cl$^-$.

PXRD

In order to better characterise the complex phase obtained from **L1***, we performed a high-resolution PXRD measurement. The experimental powder pattern was compared with those calculated from the single-crystal data of **1** and **3** (see Fig. 11). Unit cell parameters of the phase obtained from **L1*** refined in cubic cell approximation with Le Bail method (a = 27.7026(8) Å, V = 21,259.9(10) Å^3, see Supporting Information) are close to parameters of **1** (a = 27.711(5) Å, V = 21,280(6) Å^3).

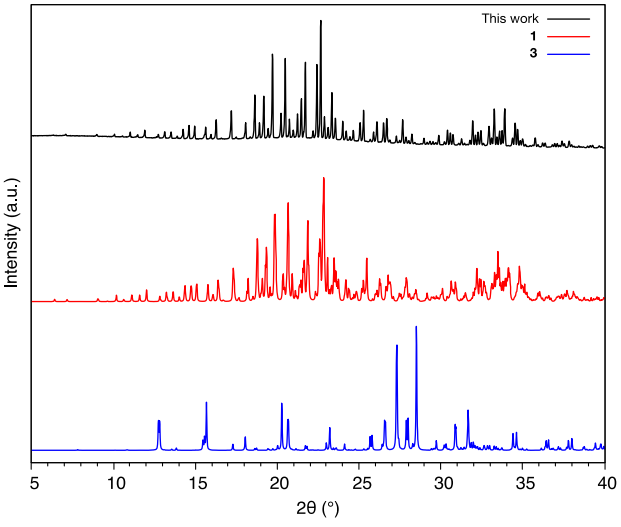

Fig. 11: Calculated powder pattern of **3** and **1**, and experimental powder patten of crystalline sample obtained in this work from **L1***.

The PXRD data confirm that the crystalline phase obtained is complex. However, it is not possible to ascertain whether the crystalline phase obtained in this work is **1**, **2** or any new FK phase of $4APH^+Cl^-$. No signal of the monohydrate phase **3** was observed.

Molecular dynamics

A simulation box was filled with 1000 $4APH^+Cl^-$ ion pairs, 1040 water molecules and 680 acetone molecules, to respect the experimental ratio found in the solutions from which crystalline phases were grown. Details of the simulation protocol and Force Field parameters can be found in the Experimental section and Supporting Information. One of the key results that is obtained from the simulation is the structure of the solvation shell of the $4APH^+$ cation. In Fig. 12 we show the Radial Distribution Function g(*r*) between the $4APH^+$ and chloride, water and acetone, respectively. In order to integrate the g(*r*) to count the number of molecules surrounding the $4APH^+$ moiety, we selected the most internal atoms of the molecules. The carbon bonded to the amino group (C4) and chloride, water oxygen and carbonyl carbon of acetone, were chosen, respectively. Together with the RDF we also show the integral number of molecules contained in a spherical shell, up to a given radius.

Figure 12 clearly shows that water and chloride are approximately equivalent, in terms of population of the $4APH^+$ solvation shell, while acetone is significantly lower. For example, at r = 7.6 Å, the average number of chloride and water molecules in the solvation shell of 4AP is exactly the same (6.9), while the average number of acetone molecules is 3.5, that is slightly lower than the bulk composition. The number of $4APH^+$ molecules surrounding a given cation is comparable with those of acetone, at short distances.

More insights can be obtained from the spatial distribution function which give a qualitative description of where the different molecules of the first solvation shell are actually located, with respect to the aromatic ring of $4APH^+$. These are shown in Fig. 13. The results of the simulation show the different tendency of acetone and water to interact to the $4APH^+$ cation and coordinate it. As it may be expected, the oxygen of water interacts directly with the positively-charged groups of cation, i.e. with NH and NH_2 moieties. A similar interaction is obviously observed also in the case of Cl^-. Interestingly, both the water and the Cl^- do not interact specifically with the aromatic ring, where acetone and the pyridinium are found. Hence, it is clear that the presence of acetone plays a major role in the solvation shell of cation, competing with the cation and limiting the π–π interaction which would lead to the formation of the monohydrate phase **3**.

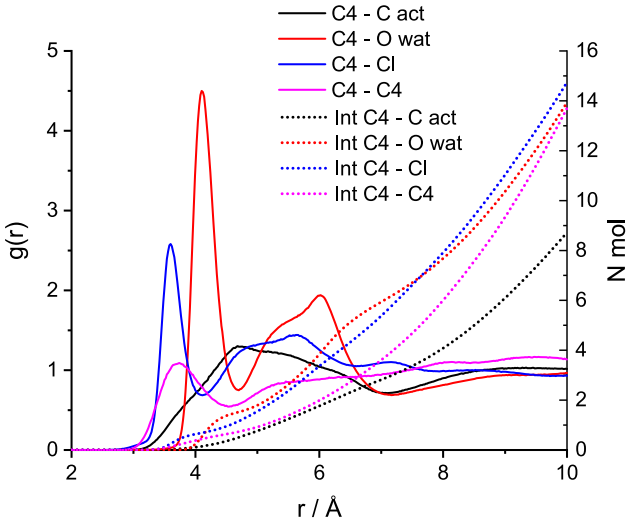

Fig. 12: (Left axis, solid lines) radial distribution functions of the distance between the amino carbon of the ring (C4) of $4APH^+$ and chloride (Cl), water oxygen (O wat), the carbonyl carbon of acetone (C act) and the amino carbon of the ring of $4APH^+$, respectively. (Right axis, dotted line): Number of molecules (chloride, water, acetone and 4AP) contained in a sphere of radius *r* and centred on C4 of $4APH^+$ as obtained from the integration of the RDF.

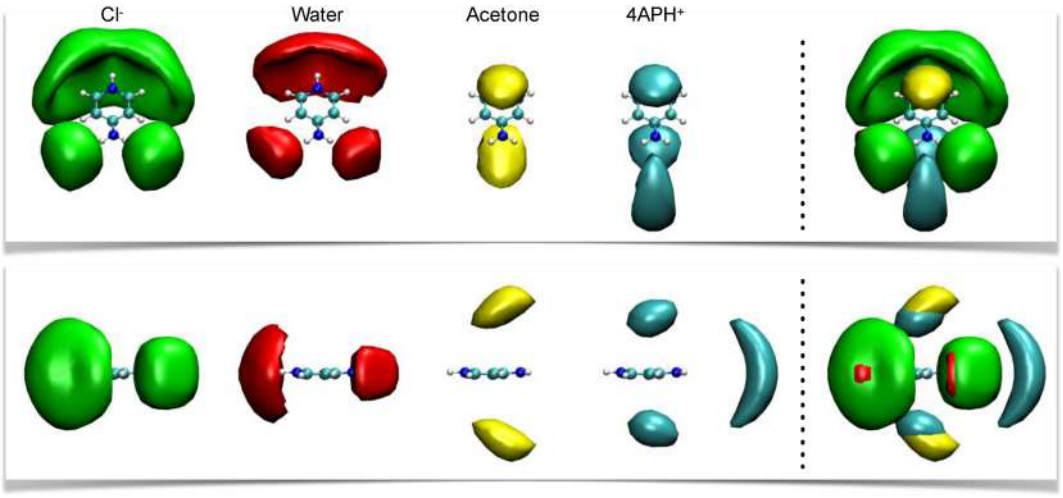

Fig. 13: Two views of spatial distribution functions around $4APH^+$ cation. SDF are shown for the Cl^- (green), water (oxygen atom, red), acetone (carbon atom of carbonyl, yellow), $4APH^+$ (carbon C4, cyan). The isodensity values are scaled proportionally to the number of molecules in the simulation box: 5.200 for Cl^- and $4APH^+$, 5.408 for water and 3.536 for acetone.

Conclusions

This work extends the knowledge on the crystallisation of complex FK phases of the simple chloride salt of 4-amino-pyridine from water, adding acetone as the antisolvent. With respect to our previous work on FK phases, we defined a new preparation of the DLP precursor of the FK phases, obtained directly from water, by diffusing acetone. Also in this case, we observed an LLPS that resulted in the separation of a DLP, from which crystals were obtained. Solid-state characterisation of these was carried out by NMR as well as by PXRD. Although the results provided evidence that the crystalline phase obtained from water upon the addition of acetone is a complex Frank–Kasper structure, the results acquired so far do not allow yet to ascertain whether significant differences with respect to the previously reported FK phases exist.

We investigated the DLP by liquid NMR experiments, to ascertain if any differences with the previous system could be observed and, most importantly, to investigate the role of acetone in promoting the crystallisation of these phases. The results from liquid-state NMR provided information about the composition of solutions after LLPS and prior crystallisation. In addition, the heteronuclear NMR characterisation highlighted the tendency of the system to aggregate and form strong H-bonds. The characterisation of the DLP by NOESY and ROESY experiments showed that these aggregates interact with both water and acetone, suggesting that acetone has a more specific role in the crystallisation of these phases, other than locally increasing the supersaturation and promoting the nucleation.

This hypothesis was confirmed by the results of classical MD simulation. MD calculations confirm that acetone is present in the first solvation sheath of the cation, occupying the positions on the top and the bottom of the aromatic ring of $4APH^+$. We believe this specific interaction is the reason why in the presence of acetone, instead to nucleate as the simple monohydrate, $4APH^+Cl^-$ forms the complex FK phases. In our opinion, the acetone-$4APH^+$ interaction competes with the π–π stacking between cations, which represents the most important interaction observed in the monohydrate phase. As water is removed from the system, $4APH^+Cl^-$ pairs aggregate forming complex spherical arrangements that eventually produce the FK phases.

These results suggest that the use of different antisolvents to model the interactions between solute and solvents is a viable route, allowing to explore further the crystallisation of complex structures from simple organic salts.

Experimental

Sample preparation

The first series of experiments was carried out by dissolving commercial 4AP (1 g, 10.6 mmol) in aqueous HCl (2 mL, 12 mmol). Upon addition of 3 mL of neat acetone (40 mmol), the solution became cloudy and further addition of the antisolvent induced an LLPS. When about 60 mL of neat acetone were added, the DLP on the sides of the vial crystallised. Block-like single crystals were also grown from the DLP on the bottom of the vial after approximately 36 h. The shape of the crystals was similar to those of **1**, and needle-like crystals of **3** were not observed.

The second series of experiments was carried out by dissolving a larger amount of 4AP (10 g, 106 mmol) in aqueous HCl (20 mL, 120 mmol). Upon addition of 40 mL of neat acetone (400 mmol), the solution became cloudy and further addition of the antisolvent induced an LLPS. When about 1 L of neat acetone was added, the DLP on the sides of the glass bottle crystallised. Block-like single crystals were grown, similarly to the previous crystallisation on a smaller scale.

NMR characterisation

The NMR spectra of solutions were recorded lock-on, using a spectrometer operating at 9.4 T (400 MHz for ^{1}H), using a 5-mm broadband probe with temperature regulation. The NMR spectra were generally recorded at 25 °C, unless stated otherwise.

The spectra of quadrupolar nuclei (^{14}N, ^{17}O, ^{35}Cl, ^{37}Cl) were recorded using the RIDE pulse sequence, which we previously used to reduce baseline distortions due to acoustic ringing [26]. The relaxation delay and the acquisition time were ranging between 5 and 25 ms; the number of transients was adapted according to the signal-to-noise ratio. The processing comprised exponential multiplication of the free induction decay with a line broadening factor of a few Hz, correction of the first points by a backward linear prediction for removal of the residual acoustic ringing, zero filling prior to Fourier transform, phase, and baseline corrections.

The ^{1}H chemical shift scale was referenced to the signal of the internal DSS standard (0.0 ppm). The $^{35/37}$Cl spectra were referenced to NaCl solution (0.0 ppm) in D_2O, which was in a coaxial tube. ^{17}O spectra were referenced to D_2O, which was in a coaxial tube. ^{14}N was referenced to an external aqueous saturated solution of ammonium chloride (25.3 ppm) [27].

The ^{13}C SSNMR spectra were recorded at room temperature using a JEOL ECZ-R spectrometer operating at 14.1 T (^{13}C frequency = 150.9 MHz) equipped with a 3.2 mm AUTOMAS probe. The samples were packed in 3.2 mm zirconia rotors and spun at 10 kHz. The number of transients was about 5000. The relaxation delay was set to 5 s and the contact time was equal to 2 ms. Chemical shifts were referenced externally to the ^{13}C chemical shift of adamantane (38.48 ppm). SPINAL-64 ^{1}H decoupling with an rf-field of 88 kHz was applied during the FID.

PXRD

A 0.5 mm diameter capillary was filled with the sample obtained from **L1***. A high-resolution PXRD pattern was collected at room temperature (around 295 K) in transmission mode with an STOE STADI MP diffractometer (generator tension and current of 40 kV and 40 mA), between 2.000 and 60.395° 2θ angle with a step size of 0.15°. Le Bail refinement was performed using FullProf Suite [28].

MD simulations

Simulations were run with the software package Gromacs 2019 [29, 30]. The Force Field parameters were taken from the OPLS [31, 32] FF except for the partial atomic charges, see Supporting Information. The simulation box contained 1000 ion pairs, 680 acetone molecules and 1040 water molecules (for a total of 24,920 atoms). All bonds were constrained by the LINCS algorithm [33]. The leap-frog integrator was used with a time step of 1 fs and a cut-off of 10 Å for the van der Waals and short-range electrostatic interaction. The Particle-Mesh-Ewald (PME) [34] technique was used to handle long-range electrostatic interaction with an interpolation order of 4. Simulations were run in the NPT ensemble using the Berendsen thermostat and barostat [35] with applied isotropic periodic boundary conditions. Additional details can be found in Supporting Information.

Acknowledgments: The authors acknowledge the PC^2 platform of the University of Namur for access to NMR and XRD facilities. LF acknowledges the National Fund for Scientific Research – FNRS, for the CDR Research Credit (NMR COMPASS, Application ID: 40007887 and the Large Equipment Call (Application ID: 32904189). Calculations were run on the CINECA parallel supercomputers thanks to ISCRA projects nr. HP10B8AOVV. We also thank the C3P community of the Department of Chemical Sciences of the University of Padova for the allocation of computational time.

References

[1] J. Chen, B. Sarma, J. M. B. Evans, A. S. Myerson. *Cryst. Growth Des*. **11**, 887 (2011), https://doi.org/10.1021/cg101556s.
[2] J. Lombard, V. J. Smith, T. le Roex, D. A. Haynes. *CrystEngComm* **22**, 7826 (2020), https://doi.org/10.1039/d0ce01470b.
[3] R. Montis, M. B. Hursthouse, J. Kendrick, J. Howe, R. J. Whitby. *Cryst. Growth Des*. **22**, 559 (2022), https://doi.org/10.1021/acs.cgd.1c01132.
[4] R. J. Davey, K Allen, N Blagden, WI Cross, HF Lieberman, MJ Quayle. *CrystEngComm* **4**, 257 (2002), https://doi.org/10.1039/b203521a.
[5] A. v Dighe, P. K. R. Podupu, P. Coliaie, M. R. Singh. *Cryst. Growth Des*. **22**, 3119 (2022), https://doi.org/10.1021/acs.cgd.2c00014.
[6] R. Miller, J. Sefcik, L. Lue. *Cryst. Growth Des*. **22**, 2192 (2022), https://doi.org/10.1021/acs.cgd.1c01269.
[7] G. Saielli, A. Bagno. *Phys. Chem. Chem. Phys.* **12**, 2981 (2010), https://doi.org/10.1039/b922550a.
[8] C. Moreau, G. Douhéret. *Thermochim. Acta* **13**, 385 (1975), https://doi.org/10.1016/0040-6031(75)85079-9.
[9] C. Moreau, G. Douhéret. *J. Chem. Thermodyn*. **8**, 403 (1976), https://doi.org/10.1016/0021-9614(76)90060-4.
[10] G. Douhéret, C. Moreau, A. Viallard. *Fluid Phase Equilib*. **22**, 289 (1985), https://doi.org/10.1016/0378-3812(85)87028-x.
[11] B. Kežić, A. Perera. *J. Chem. Phys*. **137**, 134502 (2012), https://doi.org/10.1063/1.4755816.
[12] L. de V. Engelbrecht, F. Mocci, Y. Wang, S. Perepelytsya, T. Vasiliu, A. Laaksonen. Molecular perspective on solutions and liquid mixtures from modelling and experiment. In *Soft Matter Systems for Biomedical Applications*, L. Bulavin, N. Lebovka (Eds.), pp. 53–84, Springer, Cham (2022).
[13] A. Bagno, F. Rastrelli, G. Saielli. *Prog. Nucl. Magn. Reson. Spectrosc*. **1**, 41 (2005), https://doi.org/10.1016/j.pnmrs.2005.08.001.
[14] R. Montis, L. Fusaro, A. Falqui, M.B. Hursthouse, N. Tumanov, S. J. Coles. *Nature* **590**, 275 (2021), https://doi.org/10.1038/s41586-021-03194-y.
[15] E. D. Sloan. *Nature* **426**, 353 (2003), https://doi.org/10.1038/nature02135.
[16] T. D. W. Claridge. in *High-resolution NMR techniques in organic chemistry*, **27**, Elsevier, Amsterdam (2016).
[17] A. G. Avent, P. A. Chaloner, M. P. Day, K. R. Seddon, T. Welton. *J. Chem. Soc., Dalton Trans.* **23**, 3405 (1994), https://doi.org/10.1039/dt9940003405.
[18] B. Halle. *J. Chem. Phys*. **119**, 12372 (2003), https://doi.org/10.1063/1.1625632.
[19] D. Frezzato, F. Rastrelli, A. Bagno. *J. Phys. Chem. B* **110**, 5676 (2006), https://doi.org/10.1021/jp0560157.
[20] A. Bagno, G. Scorrano. *Acc. Chem. Res*. **33**, 609 (2000), https://doi.org/10.1021/ar990149j.
[21] M. Yudasaka, T. Sugawara, H. Iwamura, T. Fujiyama. *Bull. Chem. Soc. Jpn*. **54**, 1933 (1981), https://doi.org/10.1246/bcsj.54.1933.
[22] J. Ogino, H. Suezawa, M. Hirota. *Chem. Lett*. **12**, 889 (1983), https://doi.org/10.1246/cl.1983.889.
[23] Y. Saito. *Can. J. Chem*. **43**, 2530 (1965), https://doi.org/10.1139/v65-347.
[24] C. Wiedemann, G. Hempel, F. Bordusa. *RSC Adv*. **9**, 35735 (2019), https://doi.org/10.1039/c9ra07731f.
[25] A. L. Webber, L. Emsley, R. M. Claramunt, S. P. Brown. *J. Phys. Chem. A* **114**, 10435 (2010), https://doi.org/10.1021/jp104901j.
[26] L. Fusaro, M. Luhmer. *Inorg. Chem*. **53**, 8717 (2014), https://doi.org/10.1021/ic501324r.
[27] P. Bertani, J. Raya, B. Bechinger. *Solid State Nucl. Magn. Reson*. **61**, 15 (2014), https://doi.org/10.1016/j.ssnmr.2014.03.003.
[28] J. Rodriguez-Carvajal. *Phys. B Condens. Matter* **192**, 55 (1993), https://doi.org/10.1016/0921-4526(93)90108-i.
[29] M. J. Abraham, T. Murtola, R. Schulz, S. Páll, J. C. Smith, B. Hess. *SoftwareX* **1–2**, 19 (2015), https://doi.org/10.1016/j.softx.2015.06.001.

[30] H. J. C. Berendsen, D. van der Spoel, R. van Drunen. *Comput. Phys. Commun*. **91**, 43 (1995), https://doi.org/10.1016/0010-4655(95)00042-e.
[31] W. L. Jorgensen, D. S. Maxwell, J. Tirado-Rives. *J. Am. Chem. Soc*. **118**, 11225 (1996), https://doi.org/10.1021/ja9621760.
[32] W. L. Jorgensen, J. Tirado-Rives. *J. Am. Chem. Soc*. **110**, 1657 (1988), https://doi.org/10.1021/ja00214a001.
[33] B. Hess, H. Bekker, H. J. C. Berendsen, J. G. E. M. LINCS Fraaije. *J. Comput. Chem*. **18**, 1463 (1997), https://doi.org/10.1002/(sici)1096-987x(199709)18:12<1463::aid-jcc4>3.0.co;2-h.
[34] T. Darden, D. York, L. Pedersen. *J. Chem. Phys*. **98**, 10089 (1993), https://doi.org/10.1063/1.464397.
[35] H. J. C. Berendsen, J. P. M. Postma, W. F. van Gunsteren, A. DiNola, J. R. Haak. *J. Chem. Phys*. **81**, 3684 (1984), https://doi.org/10.1063/1.448118.

Supplementary Material: This article contains supplementary material (https://doi.org/10.1515/pac-2022-1208).